

Revisiting the magnetic structure and charge ordering in $\text{La}_{1/3}\text{Sr}_{2/3}\text{FeO}_3$ by neutron powder diffraction and Mössbauer spectroscopy

F. Li,^{1,*} V. Pomjakushin,² T. Mazet,³ R. Sibille,² B. Malaman,³ R. Yadav,⁴ L. Keller,²
M. Medarde,¹ K. Conder,¹ and E. Pomjakushina¹

¹Laboratory for Multiscale Materials Experiments, Paul Scherrer Institut, 5232 Villigen, Switzerland

²Laboratory for Neutron Scattering and Imaging, Paul Scherrer Institut, 5232 Villigen, Switzerland

³Institut Jean Lamour, UMR-CNRS 7198, Université de Lorraine, BP 70239, 54506 Vandoeuvre-lès-Nancy Cedex, France

⁴Laboratory for Scientific Developments and Novel Materials, Paul Scherrer Institut, 5232 Villigen, Switzerland



(Received 23 February 2018; revised manuscript received 30 April 2018; published 17 May 2018)

The magnetic ordering of $\text{La}_{1/3}\text{Sr}_{2/3}\text{FeO}_3$ perovskite has been studied by neutron powder diffraction and ^{57}Fe Mössbauer spectroscopy down to 2 K. From symmetry analysis, a chiral helical model and a collinear model are proposed to describe the magnetic structure. Both are commensurate, with propagation vector $\mathbf{k} = (0,0,1)$ in $R\bar{3}c$ space group. In the former model, the magnetic moments of Fe adopt the magnetic space group $P3_221$ and have helical and antiferromagnetic ordering propagating along the c axis. The model allows only a single Fe site, with a magnetic moment of $3.46(2)\mu_B$ at 2 K. In the latter model, the magnetic moments of iron ions adopt the magnetic space group $C2/c$ or $C2'/c'$ and are aligned collinearly. The model allows the presence of two inequivalent Fe sites with magnetic moments of amplitude $3.26(3)\mu_B$ and $3.67(2)\mu_B$, respectively. The neutron-diffraction pattern is equally well fitted by either model. The Mössbauer spectroscopy study suggests a single charge state $\text{Fe}^{3.66+}$ above the magnetic transition and a charge disproportionation into $\text{Fe}^{(3.66-\zeta)+}$ and $\text{Fe}^{(3.66+2\zeta)+}$ below the magnetic transition. The compatibility of the magnetic structure models with the Mössbauer spectroscopy results is discussed.

DOI: [10.1103/PhysRevB.97.174417](https://doi.org/10.1103/PhysRevB.97.174417)

I. INTRODUCTION

The $R_{1/3}\text{Sr}_{2/3}\text{FeO}_3$ (R = rare earth) family is reported to show a crossover between localized and itinerant behavior by variation of the size of the rare-earth ion [1]. For R = La, Pr, and Nd, a $2\text{Fe}^{4+} \rightarrow \text{Fe}^{3+} + \text{Fe}^{5+}$ charge disproportionation (CD) accompanied by $\text{Fe}^{3+}/\text{Fe}^{5+}$ charge ordering (CO), a magnetic ordering, and a metal-insulator (MI) transition was reported to occur at 200, 180, and 165 K, respectively. For smaller rare-earth ions no MI transition is observed, the compounds being purely insulating below room temperature.

The MI transition for R = La, Pr, and Nd was explained by CD and CO. For R = La, the CO was found to occur by using Mössbauer spectroscopy [2] and electron microscopy [3]. On the basis of the CO sequence $\dots\text{Fe}^{5+}\text{-Fe}^{3+}\text{-Fe}^{3+}\dots$, the magnetic structure of this compound was reported to be $P\bar{3}m1$ [4] or $P1$ [5] from the neutron-diffraction studies performed at 50 and 15 K, respectively. The former seems not to be a correct solution since the presence of rotoinversion $\bar{3}$ is incompatible with the claimed collinear magnetic structure, with the collinear moments in the ab plane in $R\bar{3}c$ metric; and the latter might be a correct solution, but without any symmetry restrictions in space group $P1$. Moreover, the presence of Fe^{5+} below T_{MI} is not consistent with the x-ray-absorption data [6], and resonant x-ray scattering measurements indicate that the CD is not significant [7]. Furthermore, the R = Eu sample is reported to have a change of Mössbauer response across the magnetic ordering transition similar to that of the

R = La compound [8], which is surprising given the absence of MI transition. The change of the Mössbauer response for both compounds was then ascribed to the long-range magnetic ordering with two types of magnetic interactions [9]. Therefore the magnetic structure and the associated change of Mössbauer spectra are still not well understood.

In this paper we report neutron powder-diffraction and Mössbauer spectroscopy studies in the temperature range 2–300 K for $\text{La}_{1/3}\text{Sr}_{2/3}\text{FeO}_3$. New models of magnetic structure are presented and their general implications and compatibility with the results of a local probe technique, ^{57}Fe Mössbauer spectroscopy, are discussed.

II. EXPERIMENTAL DETAILS

The polycrystalline sample used in this study was prepared by solid-state reactions. Stoichiometric amounts of dried La_2O_3 , SrCO_3 , and Fe_2O_3 were mixed thoroughly by hand in an agate mortar, placed in an alumina crucible, and annealed at 1473 K for 40 h in a muffle furnace in the air. The obtained powder was then ground, pressed into a pellet, and sintered at 1673 K for 40 h. The sintering was repeated once with intermediate grinding. To ensure the oxygen stoichiometry, the sample was further annealed under oxygen flow at 873 K for 72 h. Phase purity was checked by laboratory x-ray powder diffraction. The oxygen content was verified by thermogravimetric H_2 reduction analysis performed on a Netzsch model STA 449C analyzer. Resistivity and bulk magnetic properties were measured using a Quantum Design physical property measurement system. The resistivity was measured on cooling

*fei.li@psi.ch

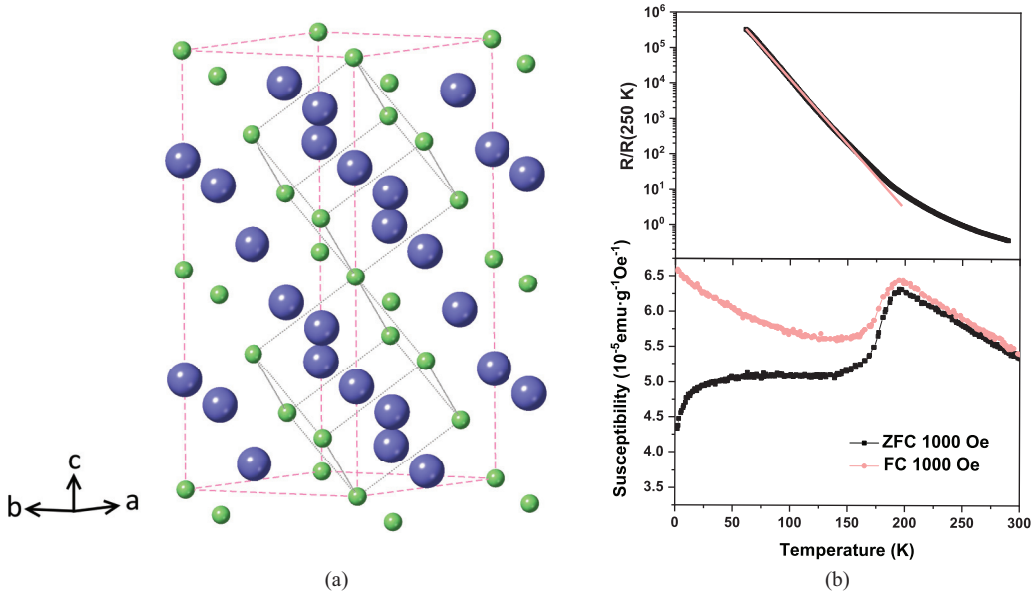


FIG. 1. (a) The crystal structure of $\text{La}_{1/3}\text{Sr}_{2/3}\text{FeO}_3$. The rhombohedral space group $R\bar{3}c$ is shown in hexagonal setting (the unit cell in pink dotted lines) and rhombohedral setting (the unit cell in grey dotted lines). The hexagonal [001] is equivalent to the rhombohedral [111]. Purple balls denote La or Sr atoms and green balls denote Fe atoms. For clarity, oxygen atoms are not shown. (b) The temperature evolution of resistivity and magnetic susceptibility. The straight line drawn in the resistivity plotting is a guide to the eye.

and subsequently heating using the four-probe method. The magnetic susceptibility was measured using zero-field-cooled (ZFC) and field-cooled (FC) protocols.

The neutron-diffraction data were collected at the Swiss Spallation Neutron Source (SINQ), Paul Scherrer Institute. Approximately 1 g of sample powder was loaded into a 6-mm-diameter vanadium can and the measurements were performed on the High-Resolution Powder Diffractometer for Thermal Neutrons (HRPT) [10] using $\lambda = 1.89$ and 1.15 Å at 230 and 2 K, and on the Cold Neutron Powder Diffractometer (DMC) using $\lambda = 2.46$ Å at a series of temperatures between 300 and 1.7 K. An absolute comparison on the 10^{-3} level of crystal lattice parameters obtained from these two instruments is not possible, because of systematic uncertainties related to wavelength calibration and peak shape parameters. The neutron-diffraction data were analyzed by Rietveld refinement using the FULLPROF suite [11], by using its internal tables of neutron-scattering lengths and magnetic form factors. The symmetry analysis was done using the ISODISTORT tool [12], BasIreps option incorporated in the FULLPROF suite [11] and software tools of the Bilbao crystallographic server [13].

The ^{57}Fe Mössbauer spectra were recorded in transmission geometry using a constant-acceleration spectrometer with a 25-mCi ^{57}Co source in a Rh matrix. The velocity scale was calibrated with a metallic iron foil at room temperature. The data were analyzed with a least-squares fitting program assuming Lorentzian peaks in the first-order approximation [14]. Isomer shifts are given with respect to $\alpha\text{-Fe}$ at room temperature.

III. RESULTS AND DISCUSSION

A. Electric and magnetic properties

$\text{La}_{1/3}\text{Sr}_{2/3}\text{FeO}_3$ crystallizes in the $R\bar{3}c$ space group at room temperature (see Fig. 1). In Fig. 1, the temperature evolution

of the resistivity, $R(T)/R(250\text{ K})$, is presented. A change of slope is visible at about 200 K, a temperature below which the material becomes more insulating. At this temperature a charge disproportionation is expected to take place. The transition observed here is less pronounced than that reported in [1, 15] on bulk samples, but it is very similar to that seen on thin films [16]. This difference may arise from the oxygen stoichiometry of the sample. In our sample the oxygen stoichiometry is 3.02 ± 0.02 .

An antiferromagnetic (AFM)-like transition is clearly observed at $T_N \sim 200$ K in the dc magnetic susceptibility $\chi(T)$ measurement (see Fig. 1), i.e., at the same temperature where a change of the slope in $R(T)/R(250\text{ K})$ is observed. The data measured in the ZFC mode diverge from that measured in the FC mode below T_N , suggesting that at low temperatures a spin-glass state or weak ferromagnetism develops.

B. Magnetic and crystal structure

1. Symmetry analysis

The neutron powder-diffraction pattern shows the appearance of additional peaks below ~ 200 K, which we interpret as magnetic scattering given the existence of a peak in the macroscopic magnetic susceptibility at this temperature (see Fig. 1). The representation theory analysis has been performed in order to determine the magnetic structure at low temperatures, which is presented as follows.

The magnetic order is considered to be characterized by a propagation vector $\mathbf{k} = (0, 0, 1)$ in $R\bar{3}c$ metrics, as determined from the Le Bail fit. This is a model-free fit in which peak matching is tested with a certain propagation vector included as an additional phase. The propagation vector found here is the Λ point of the Brillouin zone, $\Lambda = (0, 0, g)$, where g can have any value by symmetry, i.e., in general incommensurate. In this case it is considered to be locked to $(0, 0, 1)$. It should

TABLE I. The matrices and basis vectors of the small irreducible representations for Fe in $6b$ position and $\mathbf{k} = (0,0,1)$, where $a = -\frac{1}{2} + \frac{\sqrt{3}}{2}i$, $b = -\frac{1}{2} - \frac{\sqrt{3}}{2}i$, $p = \frac{\sqrt{3}}{2} + \frac{1}{2}i$, $q = i$.

	{1 000}	{3 _{00z} ⁺ 000}	{3 _{00z} ⁻ 000}	{m _{x-xz} 00 $\frac{1}{2}$ }	{m _{x2xz} 00 $\frac{1}{2}$ }	{m _{2xxz} 00 $\frac{1}{2}$ }	Basis vector	
							Fe(0,0,0)	Fe(0,0,1/2)
Λ_1	1	1	1	1	1	1	(0,0,1)	(0,0,-1)
Λ_2	1	1	1	-1	-1	-1	(0,0,1)	(0,0,1)
							(p*, q*, 0)	(0,0,0)
Λ_3	$\begin{bmatrix} 1 & 0 \\ 0 & 1 \end{bmatrix}$	$\begin{bmatrix} a & 0 \\ 0 & b \end{bmatrix}$	$\begin{bmatrix} b & 0 \\ 0 & a \end{bmatrix}$	$\begin{bmatrix} 0 & 1 \\ 1 & 0 \end{bmatrix}$	$\begin{bmatrix} 0 & b \\ a & 0 \end{bmatrix}$	$\begin{bmatrix} 0 & a \\ b & 0 \end{bmatrix}$	(0,0,0)	(q, p, 0)
							(0,0,0)	(q*, p*, 0)
							(p, q, 0)	(0,0,0)

be noted that this is not equivalent to the Γ point (0,0,0) because of the presence of R -centering translations. In the primitive rhombohedral unit cell the propagation vector is $\mathbf{k}_p = (1/3, 1/3, 1/3)$. For $\mathbf{k} = \Lambda$ in $R\bar{3}c$ there are three possible small irreducible representations (irreps) of the \mathbf{k} -vector group: Λ_1 , Λ_2 , and Λ_3 , which are one-, one-, and two-dimensional, respectively (we use nomenclature for irreps stated in [12]). For Fe in the $6b(0,0,0)$ position the magnetic representation consists of $\Gamma_{\text{mag}} = 1\Lambda_1 \oplus 1\Lambda_2 \oplus 2\Lambda_3$. These irreps and the corresponding basis vectors are listed in Table I. The Λ_1 and Λ_2 force the spin to be directed only along the c axis and have to be rejected, because of the presence of a strong (001)-magnetic peak in our experimental data. The solution is inevitably Λ_3 . For this irrep all the basis vectors are in the ab plane. The irrep Λ_3 is two-dimensional and enters two times in the magnetic representation. This, together with the fact that \mathbf{k} vector (0,0, g) is not equivalent to (0,0,- g) by symmetry, allows us to reduce the symmetry even down to the space group $P1$. There are 14 different possible Shubnikov groups for a magnetic ordering according to irrep $mLD3$, found by ISODISTORT software. Among them there are four maximal subgroups $P3_221$, $P3_22'1$, $C2/c$, and $C2'/c'$. In the following we restrict the consideration to the maximal subgroups. There are two reasons for such restriction. First, as will be shown below, the goodness of fit for some of them is as good as a Le Bail fit. Second, the latter two groups allow two Fe sites which could be compatible with the CO. It is worthwhile to note that the trigonal space groups $P3_221$ and $P3_22'1$ have their enantiomorphic pairs that should give equivalent description, namely $P3_221$ and $P3_22'1$, respectively. The choice of space group between the pairs implies a particular domain choice. The enantiomorphic pair group corresponds to an equivalent structure related by the lost inversion center, and could have been equally used to describe the proposed magnetic structure.

2. Helical model

We first consider the most symmetric solution $P3_221$ for the irrep $mLD3$, which is generated by the order parameter (OP) direction $mLD3$ (0,0, a ,0) [12]. It fits nicely to the neutron diffraction data ($\chi^2 = 2.039$, $R_{\text{mag}} = 3.39\%$). The magnetic R factors are the same as that obtained for the Le Bail fit of the magnetic peaks where all peak intensities are treated independently. This implies that the above model cannot be improved any more. This model allows the presence

of a secondary OP from a one-dimensional irrep $mGM1+$ in addition to the primary OP of $mLD3$. This results in an additional spin component along the c axis (see Ref. [17] for the general description of the symmetry concepts). This is a very good example of the case where the combined irrep approach with the restriction coming from a particular magnetic space group consistent with the primary irrep gives a direct detection of the additional secondary component in the spin arrangement from the different irrep $mGM1+$. In the traditional approach that uses only irrep basis functions and is restricted in principle to a single irrep $mLD3$, this additional AFM canting would be impossible. The fit is considerably improved when the secondary mode $mGM1+$ is taken into account, as witnessed from the above goodness of fit indicators in comparison to $\chi^2 = 5.170$, $R_{\text{mag}} = 10.50\%$ when only a single irrep $mLD3$ is considered. The contribution from the secondary mode overlaps with that from the nuclear diffraction, but there is no correlation between them in the present case. First, due to the wide Q range and only one free structure parameter (x position of oxygen atom) all nuclear contributions are practically fixed. Second, there are some peaks with a significant contribution from c axis canting which are extinct for the nuclear phase due to $R\bar{3}c$ symmetry, for instance the (011) peak at $2\theta = 24.4^\circ$. We note that the intensity of the above peak (and the other similar ones) is also zero for the main $mLD3$ component, providing convergence of the fit with the secondary mode.

In this model, Fe cations are chirally arranged in the unit cell; all the moment directions are dictated by symmetry: the projection of the moments in the ab plane propagates helically along the c axis with \mathbf{k} vector Λ , and the moments projection on the c axis are antiferromagnetically stacked (see Fig. 2). Only a single Fe site is allowed by symmetry, with a magnetic moment of $3.46(2)\mu_B$ at 2 K (see Fig. 3). This model appears to exclude long-range CO or CD of Fe ions.

The magnetic moment of Fe obtained from the refinement of the DMC data evolves with temperature and shows a first-order-like transition at T_N . It shows no significant change below T_N . The obtained value at 40 and 20 K is respectively comparable to the averaged moment from Battle *et al.*'s study ($\sim 3.31\mu_B$ at 50 K) [4] but much higher than that of Yang and co-workers ($\sim 2.43\mu_B$ at 15 K) [5]. The lattice parameters obtained from the refinement of the DMC data show a discontinuity at T_N , which in this scenario may be ascribed to magnetostriction effects.

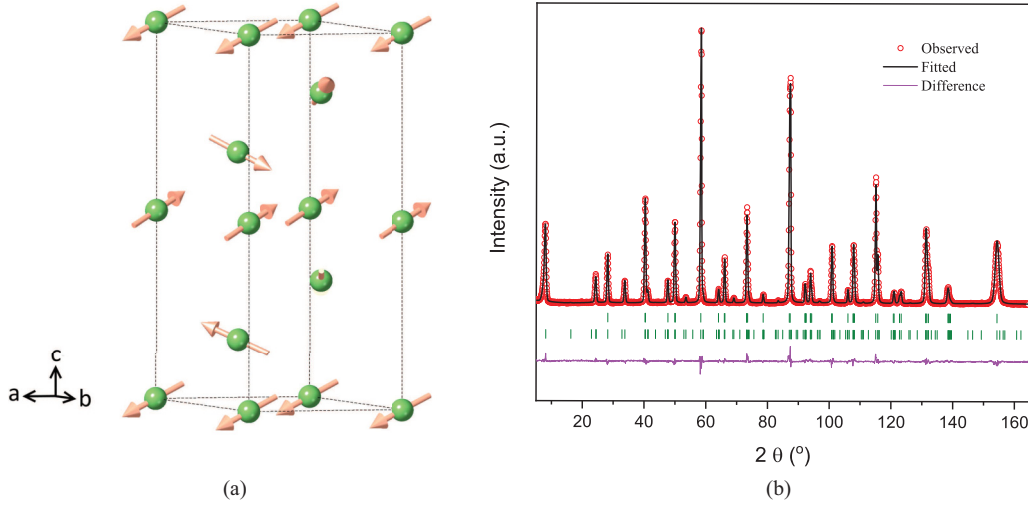


FIG. 2. (a) The helical magnetic structure of $\text{La}_{1/3}\text{Sr}_{2/3}\text{FeO}_3$ at 2 K. (b) The Rietveld refinement of the neutron-diffraction data of $\text{La}_{1/3}\text{Sr}_{2/3}\text{FeO}_3$ collected on HRPT at 2 K ($\lambda = 1.89 \text{ \AA}$), based on the helical model. The top and bottom rows of ticks below the pattern are the Bragg peak positions for the nuclear and magnetic scattering, respectively.

In the second trigonal group $P3_22'1$ the in-plane helical configuration is similar to that of $P3_221$, but the secondary spin component is $mGM2+$ [ferromagnetic (FM) along the c axis] and does not yield a convergent fit to the data.

3. Collinear model

Since CO was reported in the literature for this material [1], we studied the less symmetric model that could be compatible with CO. The maximal symmetric subgroup would be $C2/c$ and $C2'/c'$, generated by the OP direction $mLD3$ (0,0, a , a) and (a , $-a$,0,0) respectively, based on the propagation vector star $(+\Lambda, -\Lambda)$. Both groups produce a similar description of the experimental data: an amplitude modulation with two independent Fe moments. Both groups can produce the same spin configuration with however different moment direction: for $C2/c$, it is along the a axis (shown in Fig. 4) while for $C2'/c'$ it is along the b axis (not shown). The spins of Fe ions are aligned collinearly. The couplings are FM between the ions of different charge and AFM between those of the same charge. In both cases this spin configuration is generated by $mLD3$ and $mGM3+$ irreps, the latter being a secondary OP. The contribution of the Γ point is important, because it not only improves the fitting of the magnetic peaks, but also allows the proposed CO sequence. The magnetic configuration for other spin components is similar but not the same in both groups and releasing them does not give a convergent fit, as we explain below in this section. In the following we show only the results for the case of $C2/c$. The position of Fe splits up from $6b$ in $R\bar{3}c$ into $4a$ and $8f$ in $C2/c$ (see Table II). When only $mLD3$ is considered, the fitting of the magnetic peaks of the neutron-diffraction pattern at 2 K is poor ($\chi^2 = 3.093$, $R_{\text{mag}} = 9.39\%$). It gives an AFM spin configuration similar to that shown in Fig. 4, however the CO sequence as suggested from the relative moment size is $\dots\text{Fe}^{3+}\text{-Fe}^{5+}\text{-Fe}^{5+}\text{-}\dots$, which is not consistent with the previous studies [1,4,5]. The $mGM3+$ mode may give moments along the a axis. When it is taken into account, the magnetic peaks can be fitted well (see Fig. 4). The fitting yields $\chi^2 = 4.140$, $R_{\text{mag}} = 4.26\%$, slightly worse than that for the helical model. In this model, there are two Fe sites dictated by the space-group symmetry with the CO sequence $\dots\text{Fe}^{5+}\text{-Fe}^{3+}\text{-Fe}^{3+}\text{-}\dots$, where Fe^{3+} and Fe^{5+} correspond to $8f$ and $4a$ positions in $C2/c$ symmetry, respectively. The refined magnetic moment of the nominal Fe^{5+} and Fe^{3+} is $3.26(3)\mu_B$

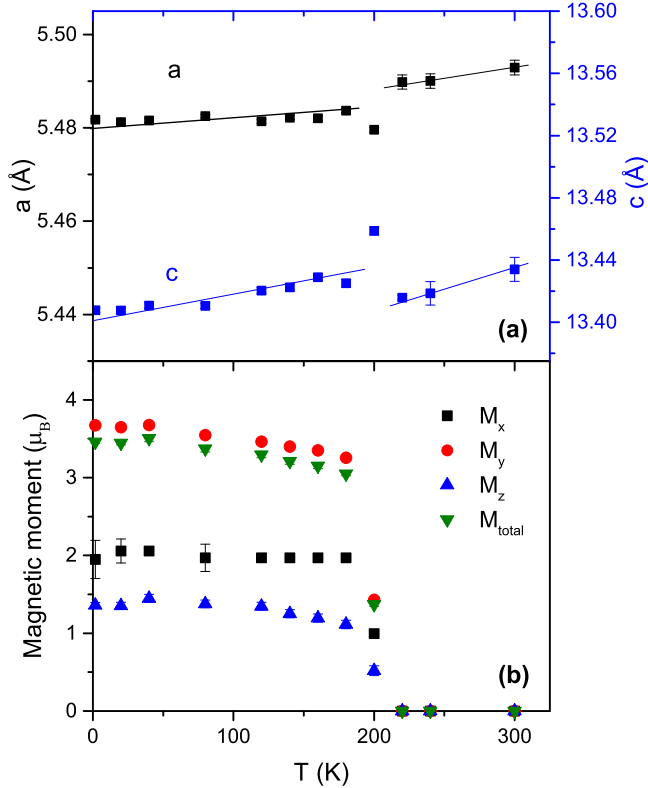


FIG. 3. The temperature evolution of (a) lattice parameters and (b) total magnetic moment and its components of Fe obtained from the Rietveld refinement of the neutron-diffraction data of $\text{La}_{1/3}\text{Sr}_{2/3}\text{FeO}_3$ collected on DMC, based on the helical model. The straight lines drawn in (a) are guides to the eye. If not visible, the error bars are smaller than the plotting symbols. See the text for details.

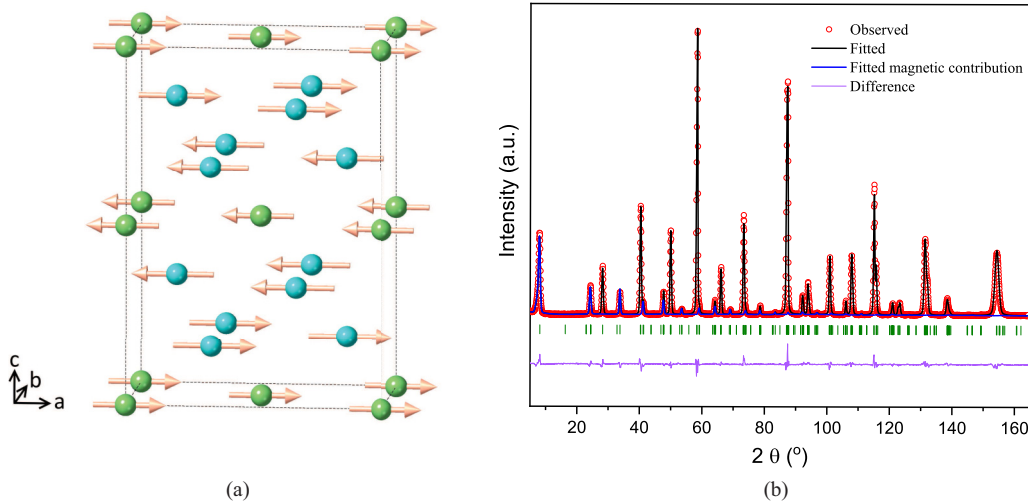


FIG. 4. (a) The collinear magnetic structure of $\text{La}_{1/3}\text{Sr}_{2/3}\text{FeO}_3$ at 2 K. The green balls denote Fe^{5+} and the blue balls denote Fe^{3+} . (b) The Rietveld refinement of the neutron-diffraction data of $\text{La}_{1/3}\text{Sr}_{2/3}\text{FeO}_3$ collected on HRPT at 2 K ($\lambda = 1.89 \text{ \AA}$), based on the collinear model. The ticks below the pattern are the Bragg peak positions for the nuclear and magnetic scattering.

and $3.67(2)\mu_B$, respectively. The average magnetic moment is $3.53\mu_B$, comparable to the value of the single moment obtained from the helical model.

We also studied in more detail the possibility to have other components for the Fe spins, and in particular the c canting similar to that in the helical model. The components of magnetic moment are possible along the a , b , and c axes in $C2/c$. The AFM configuration for Fe^{5+} and Fe^{3+} spins shown in Fig. 4 is possible only along the a axis. The component along the b axis is FM, and the component along c is AFM. In $C2/c$ group similar to $P3_221$ it is possible to have secondary symmetry modes from the Γ point $mGM3+$ (as explained above in this section) and/or $mGM1+$. The irrep $mGM1+$ gives the same AFM structure of the c component as for the helical model for both Fe1 and Fe2 sites together. We attempted to fit in this model but there was no convergence. The convergence could not be reached either when the component along the b axis was further released for refinement.

The magnetic moment on the Fe^{3+} site is larger than that on the Fe^{5+} site, but the difference in amplitude is much smaller than expected for 3+ and 5+ valences. Thus this model does not support an ideal CO, but does not exclude a partial CD. In the present case of propagation vector $\mathbf{k}_p = (1/3, 1/3, 1/3)$, the deviation of the crystal structure from the paramagnetic $R\bar{3}c$ symmetry should result in additional satellite reflections appearing at the same positions as the magnetic satellites. This makes the separation of nuclear and magnetic contributions more difficult. However the intensities of the structural satellites will not be suppressed by the magnetic form factor at large values of momentum transfer Q . A neutron-diffraction pattern measured at $\lambda = 1.15 \text{ \AA}$ allows us to go up to $Q_{\text{max}} = 11 \text{ \AA}^{-1}$. A detailed inspection of the measured pattern did not reveal the presence of any separate isolated diffraction peaks allowed in the $C2/c$ space group at high Q s (see Fig. 5). We tentatively tried to release the atomic positions in the $C2/c$ model from the ideal average positions given by the $R\bar{3}c$ paramagnetic group (see Table II), but we were not able to obtain a convergent fit.

C. Hyperfine structure

The ^{57}Fe Mössbauer spectra recorded at 300, 200, and 4 K are shown in Fig. 6. The spectrum at 300 K comprises a single broad line. Since the deviation from local cubic symmetry at the Fe site is very weak, it has been fitted using a singlet. The fitted hyperfine parameters are given in Table III. Note that fittings using a doublet yield an isomer shift ($\delta \sim 0.13 \text{ mm/s}$) identical to that when using a singlet, and a very small quadrupolar interaction ($\Delta \sim 0.12 \text{ mm/s}$) with a slightly reduced linewidth ($\Gamma \sim 0.32 \text{ mm/s}$). The spectrum recorded at 200 K, just above T_{MI} , can be fitted in the same manner as the room-temperature one. The δ value above T_{MI} lies in between that expected for Fe^{3+} and Fe^{4+} . It thus agrees with the formal charge $\text{Fe}^{3.66+}$ deduced from the chemical formula.

The spectrum recorded at 4 K comprises two sextets of unequal intensity that correspond to two Mössbauer sites, A and B. The fitted hyperfine parameters are given in Table III. They are in good agreement with those of previous Mössbauer studies [2, 18–20]. In addition, minor nonmagnetic contributions in the central part of the velocity scale were also taken into account, however they represent less than 2% of the resonant area.

The two sextets have different isomer shifts and hyperfine fields. They thus correspond to different Fe charge states. In contrast with conclusions drawn from previous Mössbauer studies [2, 18], the less intense sextet (Fe B site, $\sim 34\%$) does not correspond to the rare Fe^{5+} charge state; because its isomer shift ($\sim -0.02 \text{ mm/s}$) is not negative enough. The δ and H values are however lower than those of Fe^{4+} in SrFeO_3 ($\delta \sim 0.146$; $H \sim 33.1 \text{ T}$) [21], suggesting that site B corresponds to a noninteger charge state intermediate between Fe^{4+} and Fe^{5+} . Similarly, the hyperfine parameters of site A ($\delta \sim 0.38$; $H \sim 46.4 \text{ T}$), whose spectral weight is twice that of the Fe B site, do not correspond to that of pure Fe^{3+} as in $\alpha\text{-Fe}_2\text{O}_3$ ($\delta \sim 0.48$; $H \sim 54 \text{ T}$) [22]. This suggests that the Fe A site has also a noninteger charge state, slightly higher than trivalent. We hence conclude that the charge difference below T_{MI} is rather limited, involving

TABLE II. Crystal and magnetic structure parameters of $\text{La}_{1/3}\text{Sr}_{2/3}\text{FeO}_3$ in (a) parent paramagnetic space group $R\bar{3}c$ (no. 167, hexagonal setting) at 300 K and in magnetically ordered state at 2 K in Shubnikov magnetic space group (b) $P3_221$ (no. 154.41) or (c) $C2/c$ (no. 15.85). See the text for more details.

	(a) $R\bar{3}c$, $T = 300$ K	(b) $P3_221$, $T = 2$ K ^a	(c) $C2/c$, $T = 2$ K ^a
a (Å)	5.482 17(8)	5.477 54	9.491 62(19)
b (Å)			5.476 80(11)
c (Å)	13.405 21(23)	13.362 15	13.363 93(13)
La1/Sr1			
Wyckoff position	6a	3b	4e
x, y, z	0, 0, 1/4	1/3, 0, 1/6	0, 0, 1/4
B (Å ²)	0.686(21)		0.311(15)
La2/Sr2			
Wyckoff position		3a	8f
x, y, z		1/3, 0, 2/3	1/3, 0, -1/12
B (Å ²)			0.311(15)
Fe1			
Wyckoff position	6b	6c	4a
x, y, z	0, 0, 0	1/3, 0, 11/12	0, 0, 0
B (Å ²)	0.441(18)	0.217	0.202(13)
$M_x(\mu_B), M_y(\mu_B), M_z(\mu_B)$		1.46(7), 3.67(2), 1.32(2)	3.26(3), 0, 0
Fe2			
Wyckoff position			8f
x, y, z			1/3, 0, 2/3
B (Å ²)			0.202(13)
$M_x(\mu_B), M_y(\mu_B), M_z(\mu_B)$			-3.67(2), 0, 0
O1			
Wyckoff position	18e	6c	8f
x, y, z	0.518 12(18), 0, 1/4	1/3, 0.474 10, 1/6	0.262 95, 0.262 95, 1/4
B (Å ²)	1.057(19)		0.572(12)
O2			
Wyckoff position		3b	8f
x, y, z		0.807 43, 0, 1/6	-0.070 38, 0.262 95, 7/12
B (Å ²)			0.572(12)
O3			
Wyckoff position		6c	8f
x, y, z		1/3, 0.525 90, 2/3	0.596 28, 0.262 95, -1/12
B (Å ²)			0.572(12)
O4			
Wyckoff position		3a	4e
x, y, z		0.859 23, 0, 2/3	0, 0.474 10, 1/4
B (Å ²)			0.572(12)
O5			
Wyckoff position			8f
x, y, z			1/3, 0.474 10, -1/12
B (Å ²)			0.572(12)

^aCrystal structure parameters in the Shubnikov magnetic space group are derived from the parent group, according to the basis transformation from $R\bar{3}c$ to $P3_221$ with a linear part (1,1,0), (-1,0,0), (0,0,1) and an origin shift (2/3, 2/3, 1/12) and that from $R\bar{3}c$ to $C2/c$ with a linear part (1, -1, 0), (1, 1, 0), (0, 0, 1) and an origin shift (0, 0, 0). The lattice parameters and the atomic displacement parameters B for $C2/c$ are further refined.

two iron sites with noninteger charge states $\text{Fe}^{(3.66-\zeta)+}$ and $\text{Fe}^{(3.66+2\zeta)+}$ for Fe A and Fe B, respectively. Although the Fe charge states cannot be determined precisely, we estimate $0.2 < \zeta < 0.5$. This agrees with the conclusion of the Mössbauer study in Ref. [20]. From electronic spectroscopy data,

Herrero-Martin *et al.* [7] also concluded to a modest charge segregation. However, their conclusions included that the higher charge state has twice the spectral weight of the lower one, which is not consistent with the present and past [2, 18–20] Mössbauer data.

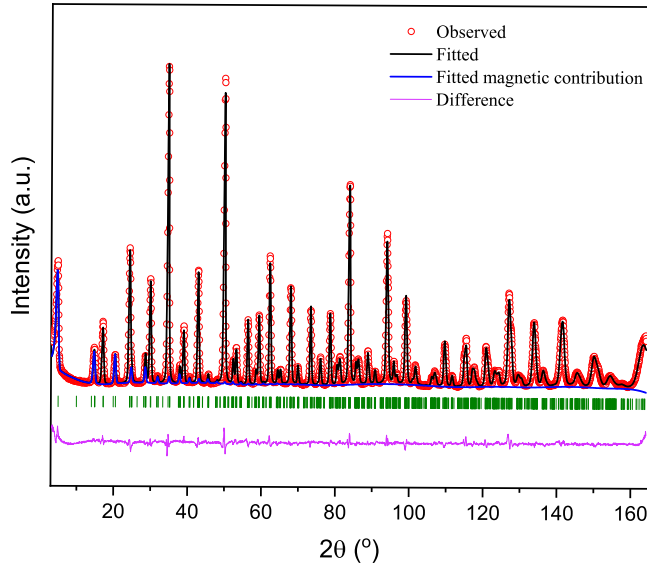


FIG. 5. The Rietveld refinement of the neutron-diffraction data of $\text{La}_{1/3}\text{Sr}_{2/3}\text{FeO}_3$ collected on HRPT at 2 K ($\lambda = 1.15$ Å), based on the collinear $C2/c$ model. The ticks below the pattern are the Bragg peak positions for the nuclear and magnetic scattering.

D. Discussion

The collinear model seems to be consistent with the present and previous results of Mössbauer spectroscopy [2,20] and the previous electron-diffraction study [3]. The Mössbauer data can be simply analyzed by considering that the $\text{Fe}^{3.66+}$ disproportionates below T_{MI} into two Fe sites: $\text{Fe}^{(3.66-\zeta)+}$ and $\text{Fe}^{(3.66+2\zeta)+}$, in the ratio 2:1. This agrees with the collinear model with the two Fe sites in $8f$ and $4a$ positions corresponding to the Mössbauer sites A and site B , respectively. However, the magnetic moments obtained from the refinement of the neutron-diffraction data are not fully consistent with the fitted hyperfine field values. The hyperfine field is built up from several contributions: the Fermi contact field (valence and core), the dipolar field, and the orbital field [23]. Although only the core contribution to the Fermi contact field scales with

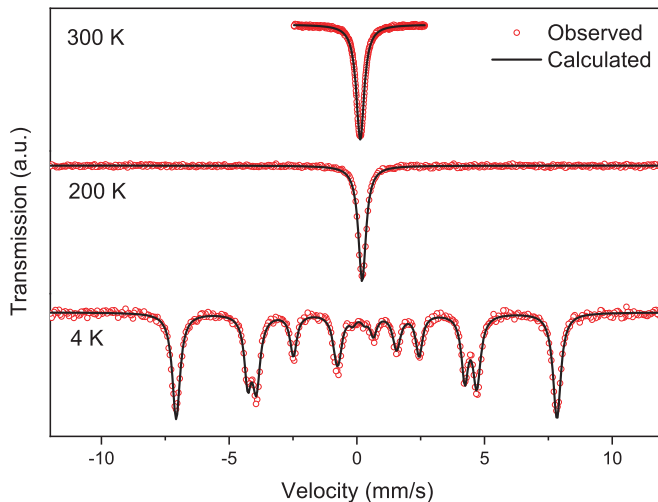


FIG. 6. The Mössbauer spectra of $\text{La}_{1/3}\text{Sr}_{2/3}\text{FeO}_3$ measured at 300, 200, and 4 K.

TABLE III. The hyperfine parameters of $\text{La}_{1/3}\text{Sr}_{2/3}\text{FeO}_3$ at 300, 200, and 4 K: linewidth Γ , isomer shift δ , apparent quadrupole splitting 2ϵ , and hyperfine field H .

	Proportion(%)	Γ (mm/s)	δ (mm/s)	2ϵ (mm/s)	H (T)
300 K	100	0.37(2)	0.13(2)		
200 K	100	0.35(2)	0.20(2)		
4 K, site A	64.9	0.36(2)	0.38(2)	0.00(2)	46.4(2)
4 K, site B	33.3	0.31(2)	-0.02(2)	0.00(2)	26.5(2)

the magnetic moment, the hyperfine field to magnetic moment ratio generally lies in the $10\text{--}15\text{-T}/\mu_{\text{B}}$ range for Fe. Hence, the Fe moment deduced from the Mössbauer hyperfine field at sites A ($8f$) and B ($4a$) lies in the range between $\sim 3.1\text{--}4.6\mu_{\text{B}}$ and $\sim 1.8\text{--}2.7\mu_{\text{B}}$, respectively. The refined magnetic moment at the $4a$ position is significantly higher ($3.26\mu_{\text{B}}$), which would imply a conversion factor as low as $\sim 8\text{ T}/\mu_{\text{B}}$.

The helical model appears inconsistent with the above results, however, it may not be fully ruled out. One possibility could be that electronic relaxations occur between two charge states at all temperatures. Relaxations are fast above the transition hence a single state is observed, while below T_{MI} , they slow down and become slower than the Mössbauer probing time (10^{-7} s) thus the two charge states are resolved. In this way, the charge separation below T_{MI} might only be apparent and only a single Fe site can be observed from neutron diffraction. The mean hyperfine field (~ 39.6 T) and the refined iron moment in the helical model ($3.46\mu_{\text{B}}$) yields a conversion factor of $\sim 11.4\text{ T}/\mu_{\text{B}}$ which lies in the commonly valid range of $10\text{--}15\text{ T}/\mu_{\text{B}}$. The other possibility could be that at low temperatures Fe cations could have two different valences locally, hence this can be probed by Mössbauer spectroscopy and electron diffraction, however the CO may not be long-ranged. Moreover the electrons are partially itinerant below T_{MI} , which implies that a short-range CO is more likely. It is also worthwhile to add that a helical model is considered to be more energetically favorable than a collinear AFM state [24,25]. A spiral structure was proposed for the spin-glass state of $\text{La}_{2-x}\text{Sr}_x\text{CuO}_4$ [25]. In $\text{La}_{1/3}\text{Sr}_{2/3}\text{FeO}_3$, such a spin-glass ground state is also possible (see Fig. 1).

Next we would like to point out some implications of the one-Fe helical model. It suggests that the first-order-like MI transition is driven purely by magnetic ordering. This is in qualitative agreement with a recent experimental observation [26]: a negative magnetoresistance and a sign reversal of the Hall effect below T_{MI} is reported for $R = \text{La}$, and the exotic low-temperature transport properties are ascribed to a consequence of the unusually long-range periodicity of the AFM ordering.

IV. SUMMARY AND CONCLUSIONS

The low-temperature magnetic structure of $\text{La}_{1/3}\text{Sr}_{2/3}\text{FeO}_3$ has been revisited and studied by neutron powder diffraction and a complementary Mössbauer spectroscopy. Based on the symmetry analysis, two crystallographic magnetic models, namely a chiral helical maximal symmetry $P3_221$ and a collinear $C2/c$ or $C2'/c'$ model, are proposed. We found both models fit equally well with the neutron-diffraction pattern

at 2 K. The less symmetric $C2/c$ or $C2'/c'$ model allows charge ordering of Fe ions but our experimental data do not show any evidence of the expected structural distortion. The Mössbauer spectroscopy results appear to support the collinear model but cannot fully rule out the helical one. The latter model suggests that the metal-insulator transition is of magnetic origin. Polarized neutron diffraction on single crystals is needed to verify the validity of either of the models.

ACKNOWLEDGMENTS

F.L. and R.Y. acknowledge the financial support from the SNSF (Schweizerischer Nationalfonds zur Förderung der Wissenschaftlichen Forschung) (Grant No. 200021_157009). R.Y. also acknowledges the financial support from Horizon 2020 (Grant No. 654000). We thank Prof. M. Kenzelmann for fruitful discussions. The work was partially performed at the Swiss Spallation Neutron Source SINQ (PSI).

-
- [1] S. K. Park, T. Ishikawa, Y. Tokura, J. Q. Li, and Y. Matsui, Variation of charge-ordering transitions in $R_{1/3}Sr_{2/3}FeO_3$ ($R = La, Pr, Nd, Sm$, and Gd), *Phys. Rev. B* **60**, 10788 (1999).
 - [2] M. Takano, J. Kawachi, N. Nakanishi, and Y. Takeda, Valence state of the Fe ions in $Sr_{1-y}La_yFeO_3$, *J. Solid State Chem.* **39**, 75 (1981).
 - [3] J. Q. Li, Y. Matsui, S. K. Park, and Y. Tokura, Charge Ordered States in $La_{1-x}Sr_xFeO_3$, *Phys. Rev. Lett.* **79**, 297 (1997).
 - [4] P. D. Battle, T. C. Gibb, and P. Lightfoot, The structural consequences of charge disproportionation in mixed-valence iron oxides. I. the crystal structure of $Sr_2LaFe_3O_{8.94}$ at room temperature and 50 K, *J. Solid State Chem.* **84**, 271 (1990).
 - [5] J. B. Yang, X. D. Zhou, Z. Chu, W. M. Hikal, Q. Cai, J. C. Ho, D. C. Kundaliya, W. B. Yelon, W. J. James, H. U. Anderson, H. H. Hamdeh, and S. K. Malik, Charge disproportionation and ordering in $La_{1/3}Sr_{2/3}FeO_{3-\delta}$, *J. Phys.: Condens. Matter* **15**, 5093 (2003).
 - [6] J. Blasco, B. Aznar, J. García, G. Subías, J. Herrero-Martín, and J. Stankiewicz, Charge disproportionation in $La_{1-x}Sr_xFeO_3$ probed by diffraction and spectroscopic experiments, *Phys. Rev. B* **77**, 054107 (2008).
 - [7] J. Herrero-Martín, G. Subías, J. García, J. Blasco, and M. Concepción Sánchez, Evidence for charge-density-wave nature of the charge-ordered phase in $La_{1/3}Sr_{2/3}FeO_3$, *Phys. Rev. B* **79**, 045121 (2009).
 - [8] Y.-J. Huang, N. Chen, G.-X. Lin, and Y.-F. Hsia, ^{57}Fe and ^{151}Eu Mössbauer study of charge disproportionation and magnetic properties in $Eu_{1/3}Sr_{2/3}FeO_3$, *J. Alloys Compd.* **474**, 229 (2009).
 - [9] J. Blasco, V. Cuartero, J. García, G. Subías, M. C. Sánchez, C. Piquer, J. Stankiewicz, J. A. Rodríguez-Velamazán, and J. Herrero-Martín, Structural, electrical and magnetic properties of $RE_{1/3}Sr_{2/3}FeO_3$ compounds ($RE = La, Pr, Nd, Eu$ and Gd), *J. Phys.: Conf. Ser.* **200**, 012015 (2010).
 - [10] P. Fischer, G. Frey, M. Koch, M. Könnicke, V. Pomjakushin, J. Schefer, R. Thut, N. Schlumpf, R. Bürge, U. Greuter, S. Bondt, and E. Berruyer, High-resolution powder diffractometer HRPT for thermal neutrons at SINQ, *Physica B* **276**, 146 (2000).
 - [11] J. Rodríguez-Carvajal, Recent advances in magnetic structure determination by neutron powder diffraction, *Physica B* **192**, 55 (1993) (also available at the website <https://www.ill.eu/sites/fullprof/>).
 - [12] B. J. Campbell, H. T. Stokes, D. E. Tanner, and D. M. Hatch, *ISODISPLACE*: A web-based tool for exploring structural distortions, *J. Appl. Crystallogr.* **39**, 607 (2006) (also available at the website <http://stokes.byu.edu/iso/isodistort.php>).
 - [13] M. I. Aroyo, J. M. Perez-Mato, D. Orobengoa, E. Tasci, G. De La Flor, and A. Kirov, Crystallography online: Bilbao crystallographic server Bulg. Chem. Commun. **43**, 183 (2011) (also available at the website <http://www.cryst.ehu.es/>).
 - [14] G. Le Caër (private communication).
 - [15] Y. M. Zhao, M. Hervieu, N. Nguyen, and B. Raveau, Charge ordering and magnetotransport transitions in $Sm_{1/3}Sr_{2/3}FeO_{3\delta}$, *J. Solid State Chem.* **153**, 140 (2000).
 - [16] J. Okamoto, D. J. Huang, K. S. Chao, S. W. Huang, C.-H. Hsu, A. Fujimori, A. Masuno, T. Terashima, M. Takano, and C. T. Chen, Quasi-two-dimensional d -spin and p -hole ordering in the three-dimensional perovskite $La_{1/3}Sr_{2/3}FeO_3$, *Phys. Rev. B* **82**, 132402 (2010).
 - [17] S. V. Gallego, J. M. Perez-Mato, L. Elcoro, E. S. Tasci, R. M. Hanson, K. Momma, M. I. Aroyo, and G. Madariaga, *MAGNDATA*: Towards a database of magnetic structures. I. The commensurate case, *J. Appl. Crystallogr.* **49**, 1750 (2016).
 - [18] P. D. Battle, T. C. Gibb, and S. Nixon, A study of charge disproportionation in the nonstoichiometric perovskite $Sr_2LaFe_3O_{8+y}$ by Mössbauer spectroscopy, *J. Solid State Chem.* **77**, 124 (1988).
 - [19] P. K. Gallagher and J. B. MacChesney, Mössbauer effect in the system $Sr_{1-x}La_xFeO_3$, *Symp. Faraday Soc.* **1**, 40 (1967).
 - [20] A. P. Chernyshev, S. A. Petrov, and N. F. Uvarov, Mössbauer spectroscopy investigation of the $La_{1/3}Sr_{2/3}FeO_{3-\delta}$ perovskite, *Phys. Solid State* **56**, 2519 (2014).
 - [21] P. K. Gallagher, J. B. MacChesney, and D. N. E. Buchanan, Mössbauer effect in the system $SrFeO_{2.5-3.0}$, *J. Chem. Phys.* **41**, 2429 (1964).
 - [22] *Mössbauer Spectroscopy*, edited by Y. Yoshida and G. Langouche (Springer-Verlag, Berlin, 2013).
 - [23] P. Novák and V. Chlan, Contact hyperfine field at Fe nuclei from density functional calculations, *Phys. Rev. B* **81**, 174412 (2010).
 - [24] B. I. Shraiman and E. D. Siggia, Spiral Phase of a Doped Quantum Antiferromagnet, *Phys. Rev. Lett.* **62**, 1564 (1989).
 - [25] A. Lüscher, A. I. Milstein, and O. P. Sushkov, Structure of the Spin-Glass State of $La_{2-x}Sr_xCuO_4$: The Spiral Theory, *Phys. Rev. Lett.* **98**, 037001 (2007).
 - [26] R. C. Devlin, A. L. Krick, R. J. Sichel-Tissot, Y. J. Xie, and S. J. May, Electronic transport and conduction mechanism transition in $La_{1/3}Sr_{2/3}FeO_3$ thin films, *J. Appl. Phys.* **115**, 233704 (2014).